Axionic and nonaxionic electrodynamics in plane and circular geometry

Iver Brevik

Department of Energy and Process Engineering, Norwegian University of Science and Technology,
N-7491 Trondheim, Norway

Amedeo M. Favitta

Department of Physics, University of Palermo, I-90123 Palermo, Italy

Masud Chaichian

Department of Physics, University of Helsinki, and Helsinki Institute of Physics,
P. O. Box 64, FI-00014 Helsinki, Finland

Various aspects of axion electrodynamics in the presence of a homogeneous and isotropic dielectric medium are discussed. First, we consider the "antenna-like" property of a planar dielectric surface in axion electrodynamics, elaborating on the treatment given earlier on this topic by Millar *et al.* [J. Cosmol. Astropart. Phys. 01 (2017) 061.]. We calculate the electromagnetic energy transmission coefficient for a dielectric plate, and compare with the conventional expression in ordinary electrodynamics. Second, we consider the situation where the medium exterior to the plate, assumed elastic, is "bent back" and glued together, so that we obtain a circular dielectric string in which the waves can propagate clockwise or counterclockwise. As will be shown, a stationary wave pattern is permitted by the formalism, and we show how the amplitudes for the two counterpropagating waves can be found. Third, as a special case, by omitting axions for a moment, we analyze the Casimir effect for the string, showing its similarity as well as its difference from the Casimir effect of a scalar field for a piecewise uniform string [I. Brevik and H. B. Nielsen, Phys. Rev. D **41,** 1185 (1990).]. Finally, including axions again we analyze the enhancement of the surface-generated electromagnetic radiation near the center of a cylindrical haloscope, where the interior region is a vacuum and the exterior region a high refractive index medium. This enhancement is caused by the curvature of the boundary, and is mathematically a consequence of the behavior of the Hankel function of the second kind for small arguments. A simple estimate shows that enhancement may be quite significant, and can therefore be of experimental interest. The presence of an absorber in the center and the possibility of adopting it to search for axions with mass in the THz region, and possibly the GHz region too, is also discussed. This proposal is suggested as an alternative to the reflector arrangement in a similar arrangement recently discussed by Liu *et al.* [Phys. Rev. Lett. **128,** 131801 (2022).].

I. INTRODUCTION

The antenna-like behavior of a single dielectric plane surface in axion electrodynamics in the presence of a strong external magnetic field is a rather remarkable phenomenon. In particular, it is quite perplexing that the Poynting vector normal to a dielectric surface is no longer continuous across the surface, a property otherwise considered as a cornerstone in electromagnetic theory. There occurs an extra

electromagnetic radiation of energy from the surface. Of course, this energy must stem from somewhere. It is rather a consequence of the interchange of field energies happening between two reservoirs, namely the usual electromagnetic reservoir, and the other one due to the axion field. A detailed exposition of these properties of axion electrodynamics is given by Millar *et al.* [1]. The effect is also planned for use in experimental broadband tests [2].

Our purpose with the present paper is first to elaborate further on some of the consequences of this dielectric-surface effect. After giving a brief survey of axion electrodynamic formalism in the next section, we consider in Sec. III the most simple dielectric system where two surfaces are involved, namely the planar dielectric disk. We point out the close similarity between the transmission

coefficients in the axion case and in the nonaxion case, a similarity that is not quite trivial. Thereafter in Sec. IV, still dealing with two-surface systems, we turn the exterior medium 2 "back" and join it with medium 1 so that we obtain a circular loop or string, and investigate if the axion formalism admits a stationary state implying clockwise and counterclockwise propagating modes. Actually the formalism does so. Such a system is most likely only of fundamental interest, but the positive outcome of the analysis demonstrates the flexibility of the axionic formalism. As a by-product, if we for a moment ignore the axion field we can calculate the electromagnetic Casimir energy of the system. This is considered in Sec. V. We show how the systems bears similarities to the piecewise uniform relativistic string which has been considered repeatedly earlier [3–9]. Finally, in Sec. VI we return to the antenna-like property of dielectric surfaces, and investigate the enhancement of the electric field near the center of a cylindrical haloscope caused by the curvature of the emitting boundary. Here the central region is a vacuum, while the outer region is a metal. The enhancement can actually be quite significant. This opens the possibility for the measurement of the emitted field from the cylindrical boundary, and may thus be an alternative to the broadband solenoidal haloscope recently proposed by Liu *et al.* [2].

Some of the pioneering papers on axion electrodynamics are listed in Refs. [10–18]. More recent works can be found in Refs. [19–43].

II. BASIC FORMALISM IN A DIELECTRIC ENVIRONMENT

We consider a pseudoscalar axion $a = a(\mathbf{r}, t)$ present in the entire universe, making a two-photon interaction with the electromagnetic field. We assume a dielectric environment where the permittivity is ε and the permeability is μ, where these material parameters are constants. The constitutive relations are $\mathbf{D} = \varepsilon\mathbf{E}$, $\mathbf{B} = \mu\mathbf{H}$. There are two field tensors, $F_{\alpha\beta}$ and $H_{\alpha\beta}$, where α and β run from 0 to 3. We assume the standard Minkowski space with the convention $g_{00} = -1$. The dual tensor is defined as $\tilde{F}^{\alpha\beta} = \frac{1}{2}\varepsilon^{\alpha\beta\gamma\delta}F_{\gamma\delta}$, with $\varepsilon^{0123} = 1$.

For convenience we give the expression for the field tensors explicitly,

$$F_{\alpha\beta} = \begin{pmatrix} 0 & -E_x & -E_y & -E_z \\ E_x & 0 & B_z & -B_y \\ E_y & -B_z & 0 & B_x \\ E_z & B_y & -B_x & 0 \end{pmatrix}, \quad (1)$$

$$H^{\alpha\beta} = \begin{pmatrix} 0 & D_x & D_y & D_z \\ -D_x & 0 & H_z & -H_y \\ -D_y & -H_z & 0 & H_x \\ -D_z & H_y & -H_x & 0 \end{pmatrix}. \quad (2)$$

The Lagrangian is

$$\mathcal{L} = -\frac{1}{4}F_{\alpha\beta}H^{\alpha\beta} + \mathbf{A} \cdot \mathbf{J} - \rho\Phi - \frac{1}{2}\partial_\mu a\partial^\mu a - \frac{1}{2}m_a^2 a^2$$
$$- \frac{1}{4}g_\gamma\frac{\alpha}{\pi}\frac{1}{f_a}a(x)F_{\alpha\beta}\tilde{F}^{\alpha\beta}. \quad (3)$$

Here, ρ and $\mathbf{J}$ are the usual electromagnetic charge and current densities (since the axions are electrically neutral they cannot contribute); g_γ is a model-dependent constant for which we adopt the value 0.36 [22]; α is the fine-structure constant, and f_a is the axion decay constant whose value is insufficiently known. Often it is assumed that $f_a \sim 10^{12}$ GeV.

Defining the combined axion–two-photon coupling constant as

$$g_{a\gamma\gamma} = g_\gamma\frac{\alpha}{\pi}\frac{1}{f_a}, \quad (4)$$

we see that the last term in the Lagrangian (3) can be written as $\mathcal{L}_{a\gamma\gamma} = g_{a\gamma\gamma}a(x)\mathbf{E} \cdot \mathbf{B}$.

It is convenient to define the quantity $\theta(x)$,

$$\theta(x) = g_{a\gamma\gamma}a(x). \quad (5)$$

Based on the expression (3), the extended Maxwell equations can then be written as

$$\nabla \cdot \mathbf{D} = \rho - \mathbf{B} \cdot \nabla\theta, \quad (6)$$

$$\nabla \times \mathbf{H} = \mathbf{J} + \dot{\mathbf{D}} + \dot{\theta}\mathbf{B} + \nabla\theta \times \mathbf{E}, \quad (7)$$

$$\nabla \cdot \mathbf{B} = 0, \quad (8)$$

$$\nabla \times \mathbf{E} = -\dot{\mathbf{B}}. \quad (9)$$

These equations are general, i.e., there are no restrictions so far on the spacetime variation of $a(x)$. The equations are moreover relativistic covariant, with respect to shift of the inertial system.

The governing equations for the fields can correspondingly be written as

$$\nabla^2\mathbf{E} - \varepsilon\mu\ddot{\mathbf{E}} = \nabla(\nabla \cdot \mathbf{E}) + \mu\dot{\mathbf{J}} + \mu\frac{\partial}{\partial t}[\dot{\theta}\mathbf{B} + \nabla\theta \times \mathbf{E}], \quad (10)$$

$$\nabla^2\mathbf{H} - \varepsilon\mu\ddot{\mathbf{H}} = -\nabla \times \mathbf{J} - \nabla \times [\dot{\theta}\mathbf{B} + \nabla\theta \times \mathbf{E}]. \quad (11)$$

The dynamical-field entities are here the electromagnetic fields; we limit ourselves to a perturbative approach in which the axions are the perturbation. We do not consider the field equations for the axions explicitly.

Assume now that a strong static magnetic field $\mathbf{B}_e = B_e\hat{\mathbf{z}}$ acts in a region where ρ and $\mathbf{J}$ are zero and the axion field is spatially uniform but varies harmonically in time,

$$a(t) = a_0 \cos \omega_a t. \tag{12}$$

This is the situation usually found in the inner region of a haloscope. Then it is convenient to separate out the part of $\mathbf{E}$ that is caused by the uniformly fluctuating axions. Calling this contribution $\mathbf{E}_a(t)$, we see from Eq. (10) that it is connected by the $\ddot{\theta}$ term. From the governing equation for $\mathbf{E}_a(t)$,

$$\nabla^2 \mathbf{E}_a - \varepsilon\mu\ddot{\mathbf{E}}_a = \mu\ddot{\theta}\mathbf{B}_e, \tag{13}$$

we then obtain, after omitting the ∇^2 term, the solution

$$\mathbf{E}_a(t) = -\frac{1}{\varepsilon} E_0 \cos \omega_a t \hat{\mathbf{z}}, \tag{14}$$

where

$$E_0 = \theta_0 B_e. \tag{15}$$

After the separation of the component $\mathbf{E}_a$, the field equation (10) takes the reduced form

$$\nabla^2 \mathbf{E} - \varepsilon\mu\ddot{\mathbf{E}} = \nabla(\nabla \cdot \mathbf{E}) + \mu\dot{\mathbf{J}} + \mu[\dot{\theta}\,\dot{\mathbf{B}} + \nabla\theta \times \dot{\mathbf{E}}]. \tag{16}$$

Likewise, for the magnetic field

$$\nabla^2 \mathbf{H} - \varepsilon\mu\ddot{\mathbf{H}} = -\nabla \times \mathbf{J}$$
$$- [\dot{\theta}\nabla \times \mathbf{B} + (\boldsymbol{\nabla}\theta)\nabla \cdot \mathbf{E} - (\nabla\theta \cdot \nabla)\mathbf{E}]. \tag{17}$$

III. ANTENNA-LIKE BEHAVIOR: TWO PLANE PARALLEL SURFACES

We begin by considering one single planar dielectric surface, placed at $x = 0$, separating the left region 1 (refractive index n_1) from the right region 2 (refractive index n_2). We assume the simple case where the media are nonmagnetic and n_1, n_2 constants and real. A strong static magnetic field $\mathbf{B}_e = B_e\hat{\mathbf{z}}$ is imposed in the z direction. An incoming wave polarized in the z direction comes in from the left, propagates in the x direction, and becomes partly reflected by the surface. The basic property following from the extended Maxwell equations in the present context is that the components of $\mathbf{E}$ and $\mathbf{H}$ parallel to the surface have to be continuous (as in ordinary electrodynamics) at $x = 0$.

This is the situation analyzed in detail by Millar *et al.* [1]. Because of the axions there will be produced two outgoing electromagnetic waves, one going to the left and one going to the right. In this sense we can consider the dielectric surface to have antenna-like properties. It does not mean that electromagnetic energy comes out from nothing, however, but that there occurs an energy interchange between the ordinary electromagnetic and the axion reservoirs.

It is now convenient, following Ref. [1], to distinguish the produced traveling fields by an extra index γ. Continuity of $\mathbf{E}_\parallel$ gives straightaway

$$E_1^\gamma + E_1^a = E_2^\gamma + E_2^a. \tag{18}$$

Next, we may take into account the relationship

$$H^\gamma = \pm\frac{1}{n} E^\gamma, \tag{19}$$

which holds for a propagating wave when the medium is nonmagnetic. This implies that the boundary condition for $\mathbf{H}_\parallel$ can be written as

$$-n_1 E_1^\gamma = n_2 E_2^\gamma, \tag{20}$$

expressing that the two wave vectors $\mathbf{k}_1$ and $\mathbf{k}_2$ are antiparallel. As $E^a = -(1/\varepsilon)E_0$, we can then solve for the produced fields to get

$$E_1^\gamma = -\frac{E_0}{n_1}\left(\frac{1}{n_2} - \frac{1}{n_1}\right), \qquad E_2^\gamma = \frac{E_0}{n_2}\left(\frac{1}{n_2} - \frac{1}{n_1}\right), \tag{21}$$

(recall that $E_0 = \theta_0 B_e$).

Remark: The argument above did not imply there to be any in-falling initial photons from the left. This is the most fundamental constellation. The argument however implies a nontrivial point, namely the use of Eq. (19) in an initial vacuum. This equation is not a general one in electrodynamics, but is implicitly resting on the assumption that there are propagating waves. This point thus brings some concern about the validity of the argument in this special case where there is initially a vacuum. Now, Millar *et al.* [1] discuss also the more general case where there are in-falling photons from the left, and in that case the use of Eq. (19) is of course nonproblematic.

Now move on to consider the situation with two dielectric surfaces; we focus first on simple dielectric slab of thickness d, surrounded by vacuum. The refractive index is $n = \sqrt{\varepsilon}$, similarly as above. It is of interest to consider the energy transmission coefficient

$$T = \left|\frac{E_T}{E_I}\right|^2 \tag{22}$$

in the presence of axions, E_T and E_I referring to the transmitted and incident wave amplitudes, respectively. Based upon Eq. (5.4a) in Ref. [1] we obtain

$$T = \frac{4n^2}{4n^2 + (n^2 - 1)^2\sin^2 kd}, \tag{23}$$

where $k = 2\pi/\lambda = n\omega$. Remarkably enough, this expression does not contain E_0. Some special cases are noteworthy: if

$d = \lambda/4$ the transmission is at minimum, $T = T_{\min} = 4n^2/(n^2 + 1)^2$, whereas if $d = \lambda/2$, the transmission is at maximum, $T = T_{\max} = 1$.

It is of interest to compare this transmission coefficient from that occurring in ordinary electrodynamics. Giving the latter quantity an extra subscript elmag, we obtain (page 514 in Stratton [44])

$$T_{\text{elmag}} = \frac{4n^2}{(n^2 + 1)^2 - (n^2 - 1)^2 \sin^2 kd}. \qquad (24)$$

It is seen that T and T_{elmag} are different, which could be expected since their derivations are different. Now, if $d = \lambda/4$, $T_{\text{elmag}} = 1$, while if $d = \lambda/2$, $T_{\text{elmag}} = 4n^2/(n^2 + 1)^2$, its minimum value. It ought to be mentioned that the reflection and transmission coefficients refer to the axion-generated fields only. If there were external probe source fields, E_{probe}, present, then its effect would be suppressed by a factor $(E_0/E_{\text{probe}})^2$.

IV. CLOSED-STRING GEOMETRY

In this section we will continue to consider dielectric systems containing two interfaces separating media of refractive indices n_1 and n_2, but now in a form that has not been considered before as far as we know. Let n_1 refer to the left medium, n_2 refer to the second medium, and assume that the media are elastic so that medium 2 can be turned back and glued to the left side of medium 1. Therewith we obtain a ring-formed system. One may ask: does such a system allow stationary oscillations to occur when axions are present? It is of physical interest to examine this point, not because of the applicability of the formalism in practice, but rather as a test of the flexibility of this kind of generalized electrodynamics. Figure 1 shows the configuration. We let σ denote the length coordinate along the string, such that the two dielectric junctions are at $\sigma = 0$ and $\sigma = L_I$. The total length of the string is $L = L_I + L_{II}$, so that the junctions $\sigma = 0$ and $\sigma = L$ are overlapping. We will be interested in the fields in the interior regions of the string. The string is lying in the xy
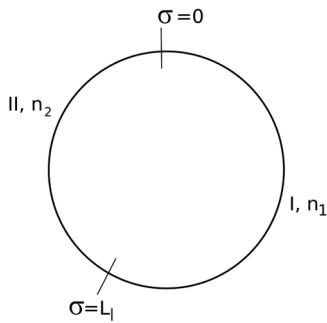

FIG. 1. Geometry and notation of the closed string.

plane, and a strong uniform magnetic field $\mathbf{B}_e$ is applied in the z direction.

We will seek stationary oscillations of the electromagnetic oscillations in the string. If $E_I(\sigma, t)$ and $E_{II}(\sigma, t)$ are the electric fields in the two regions, we have in complex representation [3]

$$E_I(\sigma, t) = e^{-i\omega t}[\xi_I e^{in_1\omega\sigma} + \eta_I e^{-in_1\omega\sigma}], \qquad (25)$$

$$E_{II}(\sigma, t) = e^{-i\omega t}[\xi_{II} e^{in_2\omega(\sigma - L_I)} + \eta_{II} e^{-in_2\omega(\sigma - L_I)}], \quad (26)$$

where ξ_I, η_I, ξ_{II}, η_{II} are constants. Analogously, using the same relationship $H = \pm nE$ as previously, we have for the magnetic field

$$H_I(\sigma, t) = n_1 e^{-i\omega t}[\xi_I e^{in_1\omega\sigma} - \eta_I e^{-in_1\omega\sigma}], \qquad (27)$$

$$H_{II}(\sigma, t) = n_2 e^{-i\omega t}[\xi_{II} e^{in_2(\sigma - L_I)} - \eta_{II} e^{-in_2\omega(\sigma - L_I)}]. \qquad (28)$$

We omit the immaterial common time-dependent factor $e^{-i\omega t}$, which is present in both (25) and (26) for the electric fields and (27) and (28) for magnetic fields (see also [3]) and introduce the shorthand notation

$$\delta_1 = n_1\omega L_I, \qquad \delta_2 = n_2\omega L_{II}. \qquad (29)$$

The boundary conditions at the junctions are, for the electric field,

$$-\frac{E_0}{\varepsilon_1} + \xi_I e^{i\delta_1} + \eta_I e^{-i\delta_1} = -\frac{E_0}{\varepsilon_2} + \xi_{II} + \eta_{II}, \quad \sigma = L_I, \quad (30)$$

$$-\frac{E_0}{\varepsilon_2} + \xi_{II} e^{i\delta_2} + \eta_{II} e^{-i\delta_2} = -\frac{E_0}{\varepsilon_1} + \xi_I + \eta_I, \quad \sigma = L, \quad (31)$$

and for the magnetic field,

$$n_1(\xi_1 e^{i\delta_1} - \eta_I e^{-i\delta_1}) = n_2(\xi_{II} - \eta_{II}), \qquad \sigma = L_I, \qquad (32)$$

$$n_1(\xi_I - \eta_I) = n_2(\xi_{II} e^{i\delta_2} - \eta_{II} e^{-i\delta_2}), \qquad \sigma = L, \qquad (33)$$

where $E_0 = \theta_0 B_e = g_{a\gamma\gamma} a_0 B_e$ as before.

Note: Similarly as in Ref. [1], in the Eqs. (25)–(33) we have assumed $\omega = \omega_a$. That is, the frequency ω of the forced oscillations has been taken to be the same as the axion frequency ω_a associated with the magnetic field $\mathbf{B}_e$. This is the most natural approach. It is however possible to take a more general approach, in which ω is assumed to be arbitrary. It means that the terms with E_0 in (30) and (31) would need to be corrected with the factor $e^{i(\omega_a - \omega)t}$. The reason for taking ω to be equal to the axion frequency ω_a is that in measurements the bulk of contribution comes from values of omega around ω_a. Indeed, the effective/measured quantities are always averages over some period of time, and the mentioned time-dependent oscillations give a delta

function when integrated over all times. If averaging over any finite period of time, the contribution of the regions of ω substantially different from ω_a due to the fast oscillating phase factor add up to zero (cf. the Lebesgue-Riemann lemma). We assume that in [1] for the same reason also such a value for ω has been chosen.

We introduce the symbol n_{12} for the refractive index ratio,

$$n_{12} = \frac{n_1}{n_2}, \tag{34}$$

and consider the scheme

$$\begin{pmatrix} e^{i\delta_1} & e^{-i\delta_1} & -1 & -1 \\ 1 & 1 & -e^{i\delta_2} & -e^{-i\delta_2} \\ n_{12}e^{i\delta_1} & -n_{12}e^{-i\delta_1} & -1 & 1 \\ n_{12} & -n_{12} & -e^{i\delta_2} & e^{-i\delta_2} \end{pmatrix} \begin{pmatrix} \xi_I \\ \eta_I \\ \xi_{II} \\ \eta_{II} \end{pmatrix}$$

$$= \begin{pmatrix} E_0(\frac{1}{\varepsilon_1} - \frac{1}{\varepsilon_2}) \\ E_0(\frac{1}{\varepsilon_1} - \frac{1}{\varepsilon_2}) \\ 0 \\ 0 \end{pmatrix}. \tag{35}$$

Here the determinant D of the system matrix M_{ik} can be calculated to be

$$\begin{aligned} D &= \det M_{ik} \\ &= -8n_{12} + 2(1 + n_{12})^2 \cos(\delta_1 + \delta_2) \\ &\quad - 2(1 - n_{12})^2 \cos(\delta_1 - \delta_2). \end{aligned} \tag{36}$$

This is a real quantity. We can now calculate explicit expressions for the field amplitudes $\xi_I, \eta_I, \xi_{II}, \eta_{II}$, in the two regions of the string. The expressions become complicated, and will not be given here. There is one particular case of interest, however, namely when n_2 becomes large in comparison to n_1 so that the ratio $n_{12} \to 0$. The lengths L_I and L_{II} are assumed arbitrary. From Eq. (36) we obtain in this case

$$\begin{aligned} D(n_{12} \to 0) &= 2\cos(\delta_1 + \delta_2) - 2\cos(\delta_1 - \delta_2) \\ &= -4\sin\delta_1\sin\delta_2, \end{aligned} \tag{37}$$

and after some calculation we obtain, as an example, the first of the amplitudes in the region $0 < \sigma < L_I$ (note that $1/\varepsilon_2 \to 0$),

$$\xi_I = \frac{E_0}{2\varepsilon_1} \left[1 - i\frac{1 - \cos\delta_1}{\sin\delta_1} \right], \qquad n_{12} \to 0. \tag{38}$$

It is noteworthy that this expression does not contain the phase δ_2 related to the length L_{II}. It is of further interest to consider the case where the length $L_I \to 0$, corresponding

to a kind of point defect sitting on an otherwise uniform string. As $\delta_1 \to 0$ in this case, we see from the last equation that

$$\xi_I = \frac{E_0}{2\varepsilon_1}, \qquad n_{12} \to 0, \qquad L_I \to 0, \tag{39}$$

which is a real quantity. If $E_0 = 0$, the axion-induced forced oscillations vanish.

In conclusion, we have managed to show that the axionic electrodynamic scheme is flexible enough to uphold stationary oscillations in the closed-string geometry.

V. CASIMIR EFFECT FOR THE CLOSED STRING

We now set $E_0 = 0$, so that the forced axion-induced oscillations vanish, and those remaining possible are only the free oscillations. They correspond to the system determinant D being zero. For a given set of geometric quantities L_I, L_{II}, n_1, n_2, the eigenfrequencies ω are thus found by solving $D = 0$ using Eq. (36). Moreover, this geometry makes it very natural to consider the Casimir effect also, after applying an appropriate regularization. This will be the topic of the present section. Actually, this situation bears a considerable similarity with the Casimir energy for the relativistic piecewise uniform string, as mentioned earlier [3–9].

For clarity, we ought to clarify the difference between the approach in Sec. IV and that of the present section in some more detail. The two cases are physically different. In Sec. IV assuming $E_0 \neq 0$, the system was exposed to forced oscillations, primarily with frequency ω_a (eventually with arbitrary ω), giving expressions for the energy E as a function of the refractive-index ratio $n_{12} = n_1/n_2$. In the present section the frequencies are no longer up to choice, but are determined by the determinant condition $D = 0$. The Casimir effect is under stationary conditions linked to discrete eigenvalues. As just mentioned, it is this condition that is just analogous to that encountered in the study of the Casimir effect for the piecewise uniform string. Before embarking on the general case, it is convenient to start with special cases of interest. The simplest case is when the string is uniform, $n_{12} = 1$, corresponding to $n_1 = n_2 = n$. Then,

$$D(n_{12} = 1) = -8(1 - \cos\omega nL), \tag{40}$$

so that the eigenfrequencies become

$$\omega_N = \frac{2\pi N}{nL}, \tag{41}$$

with $N = 1, 2, 3, \ldots$ Assuming implicitly that we apply a regularization procedure, for instance that of a cutoff regularization, we can express the Casimir energy as

$$E_{\text{uniform}} = 2 \times \frac{1}{2} \sum_{N=1}^{\infty} \omega_N, \tag{42}$$

where the factor 2 in front accounts for the degeneracy of the left-right running modes. The result is (cf., for instance, Ref. [3])

$$E_{\text{uniform}} = -\frac{\pi}{6L}. \tag{43}$$

The next special case of interest is when $n_{12} \to 0$, the case considered also in the previous section (note that the value of n_1 itself is arbitrary, not necessarily small). Then, from Eq. (37) we see that the eigenfrequencies occur in two branches,

$$\omega_N = \frac{\pi N}{n_1 L_I}, \tag{44}$$

$$\omega_N = \frac{\pi N}{n_2 L_{II}}, \tag{45}$$

again with $N = 1, 2, 3, \ldots$ (there is no degeneracy in this case, thus no extra factor 2). Introducing the symbol s for the length ratio,

$$s = \frac{L_{II}}{L_I}, \tag{46}$$

we get in this case

$$E(n_{12} \to 0) = -\frac{\pi}{24L}\left(s + \frac{1}{s} - 2\right). \tag{47}$$

This Casimir energy is in general negative, but attains its maximum value zero when the pieces have equal lengths, $s = 1$.

In the general case when n_{12} is arbitrary the situation is more complex, but can yet be handled in a reasonably simple way by making use of Cauchy's argument principle. This principle states that any meromorphic function $g(\omega)$ satisfies the equation

$$\frac{1}{2\pi i} \oint \omega \frac{d}{d\omega} \ln g(\omega) d\omega = \sum \omega_0 - \sum \omega_{\text{poles}}, \tag{48}$$

where ω_0 are the zeros and ω_{poles} are the poles of $g(\omega)$ inside the contour of integration. This contour is taken to be a semicircle of large radius R in the right half plane. A definite advantage of this method is that the multiplicities of zeros and poles are automatically included. The argument principle was introduced in connection with the Casimir effect by van Kampen *et al.* [45], and has later been made use of extensively (cf., for instance, Refs. [5,8,8,46]).

For the function $g(\omega)$ it is natural to start from the expression for D in Eq. (36), but we have to normalize it in a convenient way. We first introduce a convenient parametrization which relates the pieces L_I and L_{II} to the total length L,

$$L_I = pL, \qquad L_{II} = qL, \qquad p + q = 1. \tag{49}$$

Then, define the quantity A as

$$A = \frac{1}{4}(1 + n_{12})^2 \cos[(n_1 p + n_2 q)\omega L]$$
$$- \frac{1}{4}(1 - n_{12})^2 \cos[(n_1 p - n_2 q)\omega L]. \tag{50}$$

For a uniform string, $n_{12} = 1$ $(n_1 = n_2 = n)$, we have $A = \cos(n\omega L)$. We now define $g(\omega)$ as

$$g(\omega) = \left|\frac{1 - A}{A}\right|. \tag{51}$$

With this form, the big semicircle does not contribute to the integration. Let $\omega = i\xi$, where ξ is the frequency along the imaginary axis. This Wick rotation implies that the quantity A goes into

$$A \to A(\xi) = \frac{1}{4}(1 + n_{12})^2 \cosh[(n_1 p + n_2 q)\xi L]$$
$$- \frac{1}{4}(1 - n_{12})^2 \cosh[(n_1 p - n_2 q)\xi L]. \tag{52}$$

By performing a partial integration along the imaginary axis, and observing that the positive and negative frequencies contribute equally, we obtain for the Casimir energy

$$E = \frac{1}{2\pi} \int_0^{\infty} \ln\left|\frac{1 - A(\xi)}{A(\xi)}\right| d\xi. \tag{53}$$

With our adopted normalization, we can now test the results for E calculated in special cases. To simplify the formalism somewhat, we choose $n_1 = 1$, the lowest possible value for n_1 in nondispersive theory. Then, $n_2 = 1/n_{12}$. Let us also choose $L = 1$. This implies that the expression for $A(\xi)$ becomes simpler,

$$A(\xi) = \frac{1}{4}(1 + n_{12})^2 \cosh\left[\left(p + \frac{q}{n_{12}}\right)\xi\right]$$
$$- \frac{1}{4}(1 - n_{12})^2 \cosh\left[\left(p - \frac{q}{n_{12}}\right)\xi\right]. \tag{54}$$

A. The case of a uniform string

In this case $A(\xi)|_{x=1} = \cosh \xi$ for all p, and we get

$$E_{\text{uniform}} = \frac{1}{2\pi} \int_0^\infty \ln \left| \frac{1 - \cosh \xi}{\cosh \xi} \right| d\xi. \qquad (55)$$

The integral can be calculated analytically by means of polylogarithm functions and is equal to

$$E_{\text{uniform}} = -3 \frac{\pi}{16}. \qquad (56)$$

It is worth noticing it is different from (43) by a multiplicative factor $\frac{9}{8}$. One could think that this is an inconsistency as the calculations seem to refer to the same Casimir energy E for the homogenous string. Actually, the two situations are different: The energy of Eq. (43) is calculated for a scalar field, so quantum numbers run from $N = 1$ to infinity, while Eq. (56) is calculated for the electromagnetic field, where $N = 0$ contributions are not zero. It is known in electromagnetic Casimir problems for dielectrics that both TE and TM polarizations contribute with zero frequency [47]. Although the two cases are not directly comparable, we note that the result of the integral (56) is obtained from

$$E_{\text{uniform}} = -\frac{1}{2\pi}(4\text{Li}_2(1) - \text{Li}_2(-1)), \qquad (57)$$

where the first term in brackets gives the energy (43), and the second term gives the difference.

B. The case when $p = 1/2$

The string is then divided into two equal halves, the refractive-index ratio n_{12} being arbitrary. Now

$$A(\xi)|_{p=1/2} = \frac{1}{4}(1 + n_{12})^2 \cosh \left[\left(1 + \frac{1}{n_{12}}\right) \frac{\xi}{2} \right]$$
$$- \frac{1}{4}(1 - n_{12})^2 \cosh \left[\left(1 - \frac{1}{n_{12}}\right) \frac{\xi}{2} \right], \qquad (58)$$

and the Casimir energy is found by inserting this expression into Eq. (53). It is not trivial to find an analytical solution for the integral (53), so we calculated it numerically by a PYTHON program. We show the resulting plot in Fig. 2.

It is worth noticing how the energy E is positive or negative depending on the value of n_{12}. For $n_{12} \lesssim 0.15$, E is positive and has a maximum at $n_{12} \approx 0.04$; for larger n_{12} the energy is negative until it reaches the value (56) for $n_{12} = 1$. In the following case for $p \to 0$ we are discussing the similarity with this case.
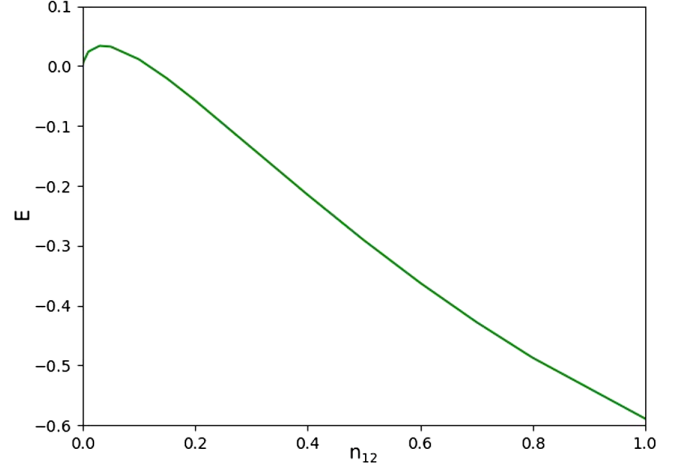

FIG. 2. Graph of E versus n_{12} in the case 2, where n_{12} is restricted to the region $0 < n_{12} < 1$. We show that E can be positive or negative depending on the value of n_{12}: for $n_{12} \lesssim 0.15$, E is positive and has a maximum at $n_{12} \approx 0.04$; for bigger n_{12} the energy is negative, until it reaches the value in Eq. (56) for $n_{12} = 1$.

C. The case when $p \to 0$

This case is of interest since it corresponds to a "particle" sitting on a uniform string. We have now $A(\xi)|_{p\to0} = n_{12} \cosh(\xi/n_{12})$, and the Casimir energy becomes

$$E = \frac{1}{2\pi} \int_0^\infty \ln \left| \frac{1 - n_{12}\cosh(\xi/n_{12})}{n_{12}\cosh(\xi/n_{12})} \right| d\xi. \qquad (59)$$

As before, we assume that n_{12} lies in the interval $0 < n_{12} < 1$. Figure 3 shows the same behavior except
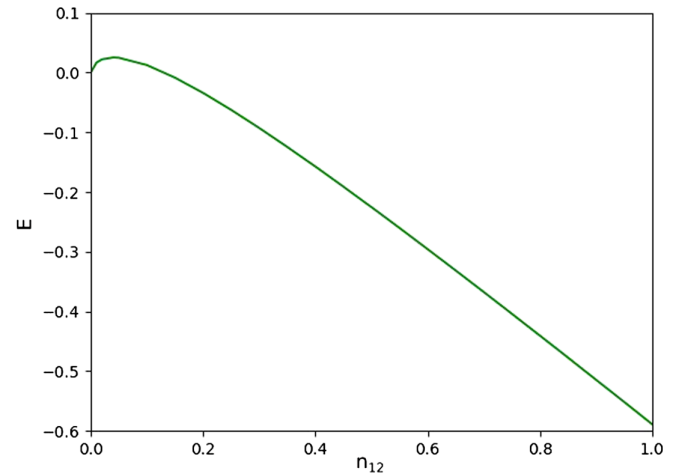

FIG. 3. Graph of E versus n_{12} in the case 3, analogous to Fig. 2. We show that E is positive or negative depending on the value of n_{12}: for $n_{12} \lesssim 0.15$, E is positive and has a maximum at $n_{12} \lesssim 0.04$; for larger n_{12}, the energy is negative until it reaches Eq. (56) for $n_{12} = 1$. The main difference from Fig. 2 relies on the behavior of the function in the middle region, where the energy of case 3 diminishes more slowly than in the case 2.

from the middle region $0.15 \lesssim n_{12} < 1$, where the energy of case 3 diminishes slower than in case 2. These similarities in the extremes for $n_{12} \lesssim 0.15$ and $n_{12} = 1$ can be understood. It is easy to verify that the integrals in Eqs. (58) and (59) give the same result for $n_{12} = 0$, because we have no fields due to boundary conditions and the medium in region II behaving as a perfect mirror so we get $E = 0$. The same is valid for $n_{12} = 1$, as the cases 1, 2, and 3 are equivalent when the string is uniform.

VI. CURVATURE-INDUCED ENHANCEMENT OF THE PRODUCED ELECTRIC FIELD AT A DIELECTRIC BOUNDARY

As our last topic, we will return to the cylindrical haloscope idea, emphasizing a point that to our knowledge has not been considered before. Namely, the extra produced electric field E^γ occurring in the interior cylindric vacuum region will necessarily be enhanced near the center of the cylinder. The enhancement is solely caused by the curvilinear geometry. Obviously, this is a point that can be of experimental interest. We assume the case when the optical frequency is equal to the axion frequency ω_a.

As before, assume there is an infinitely long cylindrical vacuum region with radius R, surrounded by an exterior massive dielectric environment of high refractive index. There is moreover a strong uniform static magnetic field $\mathbf{B}_e$ in the z direction. We assume there are only the time-varying axions present in the system, together with the extra photons E^γ that they generate at the boundary. The solutions of the Bessel equations in the exterior and interior regions are cylinder functions. No propagation of electromagnetic modes are assumed to take place in the z direction, and we can start from the usual electromagnetic mode expressions for the axial electric and the azimuthal magnetic field components in the exterior and interior regions (cf. Ref. [44], page 525)

$$E_z^{\text{ext}} = H_0^{(1)}(k_2 r) a_{\text{ext}} e^{-i\omega t}, \quad H_\theta^{\text{ext}} = i n_2 H_0^{(1)'}(k_2 r) a_{\text{ext}} e^{-i\omega t},$$
(60)

$$E_z^{\text{int}} = J_0(\omega r) a_{\text{int}} e^{-i\omega t}, \quad H_\theta^{\text{int}} = i J_0'(\omega r) a_{\text{int}} e^{-i\omega t}. \quad (61)$$

Here k_1 is the wave number in the inner region $0 < r < R$, and k_2 refers to the outer region $r > R$. $H_p^{(1)}$ is the Hankel functions of the first kind, of order p. Azimuthal symmetry is assumed, so that only $p = 0$ applies. Outgoing waves are assumed on the outside, and on the inside a stationary wave field is assumed, finite at the center.

In the present case the situation is different, as the antenna-like property of the boundary $r = R$ causes radiation to occur inward also. It is illustrative here to give some of the mathematical background [44]. In general, the complex Hankel functions of the first and the second kinds are defined as

$$H_p^{(1)}(\rho) = J_p(\rho) + i N_p(\rho), \quad H_p^{(2)}(\rho) = J_p(\rho) - i N_p(\rho),$$
(62)

where $J_p(\rho)$ and $N_p(\rho)$ are the real Bessel and Neumann functions. For large arguments $\rho \gg 1$ one has asymptotically, after multiplying with the common time factor $e^{-i\omega t}$,

$$H_p^{(1)}(\rho) = \sqrt{\frac{2}{\pi\rho}} e^{i(\rho - \frac{2p+1}{4}\pi - i\omega t)},$$

$$H_p^{(2)}(\rho) = \sqrt{\frac{2}{\pi\rho}} e^{-i(\rho - \frac{2p+1}{4}\pi + i\omega t)}. \quad (63)$$

This shows that $H_0^{(2)}$ is the correct cylinder function to use in the present case. It describes waves produced at the boundary $r = R$, moving inward.

Now, replacing J_0 by $H_0^{(2)}$ in Eq. (61), the equation takes the form

$$E_z^{\text{int}} = H_0^{(2)}(\omega r) a_{\text{int}} e^{-i\omega t},$$

$$H_\theta^{\text{int}} = i H_0^{(2)'}(\omega r) a_{\text{int}} e^{-i\omega t}. \quad (64)$$

As before, $k_2 = n_2\omega$ with n_2 real. The coefficients a_{ext} and a_{int} are determined by the boundary conditions at $r = R$. Looking back at the treatment in Sec. III, we will require the correspondence

$$E_2^\gamma \to H_0^{(1)}(k_2 R) a_{\text{ext}} e^{-i\omega t},$$

$$E_1^\gamma \to H_0^{(2)}(\omega R) a_{\text{int}} e^{-i\omega t}. \quad (65)$$

We assume in the following that the radius R is so large that the approximate versions (63) for the Hankel functions are applicable on the boundary. As $H_0^{(1)'}(\rho) = i H_0^{(1)}(\rho)$, $H_0^{(2)'}(\rho) = -i H_0^{(2)}(\rho)$, we can write the boundary conditions as

$$H_0^{(1)}(k_2 R) a_{\text{ext}} - \frac{E_0}{\varepsilon_2} = H_0^{(2)}(\omega R) a_{\text{int}} - E_0, \quad (66)$$

$$n_2 H_0^{(1)}(k_2 R) a_{\text{ext}} = -H_0^{(2)}(\omega R) a_{\text{int}}, \quad (67)$$

where $E_0 = \theta_0 B_e$, as before. The coefficients a_{ext} and a_{int} can then be found, and we can express the result as

$$H_0^{(1)}(k_2 R) a_{\text{ext}} = -\frac{E_0}{n_2}\left(1 - \frac{1}{n_2}\right), \quad (68)$$

$$H_0^{(2)}(\omega R) a_{\text{int}} = E_0\left(1 - \frac{1}{n_2}\right), \quad (69)$$

in agreement with Eq. (21) obtained for plane geometry.

We now move on to the central point in this analysis, which is to observe the behavior of the inward-emitted electric field E_z near the center of the cylinder. As the magnitude of $H_0^{(2)}(\rho)$ increases logarithmically as $\rho \to 0$, there will necessarily be an enhancement of the field in this region. (Note that this enhancement is a pure focusing effect caused by the boundary $r = R$, and is not related to a divergence of the source.) One might argue that the accumulation of electric fields near $r = 0$ would lead to an unstable situation. We may avoid this, at least conceptually, by assuming there to be a perfect cylindrical absorber of small radius $r = \delta$ centered at the z axis, thus allowing for stable conditions.

Letting the inward-generated field at $r = R$ be represented by $H_0^{(2)}(\omega R)$, we may for small values of the argument ρ make use of the approximation

$$H_0^{(2)}(\rho) = J_0(\rho) - iN_0(\rho) = 1 + \frac{2i}{\pi}\ln\frac{2}{\gamma\rho}, \qquad \rho \ll 1, \quad (70)$$

with $\gamma = 1.78107$. We need only consider the magnitudes of the field expressions. Thus, the magnitudes of the fields measured at the minimum radius δ and at the cylinder radius R are related by

$$\left|\frac{E_z^\gamma(\delta)}{E_z^\gamma(R)}\right| = \left|\frac{H_0^{(2)}(\omega\delta/c)}{H_0^{(2)}(\omega R/c)}\right| = \left|\frac{1 + \frac{2i}{\pi}\ln\frac{2c}{\gamma\omega\delta}}{H_0^{(2)}(\omega R/c)}\right| \quad (71)$$

in physical units.

We make finally some numerical estimates. Take $R = 20$ cm as a reasonable value for the cylinder radius, and choose for definiteness $m_a c^2 = 10^{-4}$ eV for the axion energy, which corresponds to $\omega = 1.52 \times 10^{11}$ rad/s. Then, $\omega R/c = 1.0 \times 10^2$, thus justifying use of the approximation (63). We get $|H_0^{(2)}(\omega R/c)| = 0.080$. With the minimum radius chosen as $\delta = 100$ μm, corresponding to $\rho_{\min} = \omega\delta/c = 0.051$, it is seen that also the low-argument approximation (70) is justified. We obtain for the ratio (71)

$$\left|\frac{E_z^\gamma(\delta)}{E_z^\gamma(R)}\right| = 12.5 \times |1 + 2.0i| = 28.0. \qquad (72)$$

There occurs thus a considerable enhancement of the amplitude in the neighborhood of the cylinder center. While the numerical values above were chosen so as to satisfy the mathematical approximations, there is clearly a flexibility of choosing different parameters that can better fit experimental conditions.

We emphasize again that this enhancement is solely a geometrical focusing effect, being an extension of the theory worked out earlier [1] for plane geometry. An observation of the increased signal near $r = 0$ may be of experimental interest. The idea may be looked upon as an alternative to the idea recently put forward in Ref. [2], concerning the broadband solenoidal haloscope.

The situation discussed above is obviously an idealistic one. In practice, an accurate positioning of the absorber would be needed, and the impedance-matched absorber should be with the property of having no reflection. One may ask if there exist broadband frequency reflectionless absorbers in the THz region that might be suitable for this purpose. Perhaps the use of metamaterials turns out to be useful in this context. We may mention here the paper of Zhang *et al.* on a broadband THz absorber based on dispersion-engineered catenary coupling in dual metasurface [48]. Indeed, the authors of [48] were able to obtain an ultrabroadband THz absorber with a bandwidth range from 0.52 to 4.4 THz, thus just in the region of interest. Similar investigations, in the GHz region, are given by Chen *et al.* [49] and Chen *et al.* [50]. A general review on metamaterial absorbers is recently given by Abdulkarim *et al.* [51].

ACKNOWLEDGMENTS

[1] A. J. Millar, G. R. Raffelt, J. Redondo, and F. D. Steffen, J. Cosmol. Astropart. Phys. 01 (2017) 061.

[2] J. Liu, K. Dona, G. Hoshino, S. Knirck, N. Kurinsky, N. Malaker *et al.*, Phys. Rev. Lett. **128**, 131801 (2022).

[3] I. Brevik and H. B. Nielsen, Phys. Rev. D **41**, 1185 (1990).

[4] X. Li, X. Shi, and J. Zhang, Phys. Rev. D **44**, 560 (1991).

[5] I. Brevik and E. Elizalde, Phys. Rev. D **49**, 5319 (1994).

[6] I. Brevik, H. B. Nielsen, and S. D. Odintsov, Phys. Rev. D **53**, 3224 (1996).

[7] I. Brevik, E. Elizalde, R. Sollie, and J. B. Aarseth, J. Math Phys. (N.Y.) **40**, 1127 (1999).

[8] I. Brevik, A. A. Bytsenko, and B. M. Pimentel, *Thermodynamic Properties of the Relativistic Composite String—Expository Remarks*, Theoretical Physics 2002, Part 2 (Nova Science Publication, Hauppauge, New York, 2003), p. 117.

[9] M. Bordag and I. G. Pirozhenko, arXiv:2012.14301.

[10] R. D. Peccei and H. R. Quinn, Phys. Rev. Lett. **38,** 1440 (1977).

[11] R. D. Peccei and H. R. Quinn, Phys. Rev. D **16,** 1791 (1977).

[12] P. Sikivie, Phys. Rev. Lett. **51,** 1415 (1983).

[13] S. Weinberg, Phys. Rev. Lett. **40,** 223 (1978).

[14] J. Preskill, M. B. Wise, and F. Wilczek, Phys. Lett. **120B,** 127 (1983).

[15] L. F. Abbott and P. Sikivie, Phys. Lett. **120B,** 133 (1983).

[16] M. Dine and W. Fischler, Phys. Lett. **120B,** 137 (1983).

[17] P. Sikivie, *Axion Cosmology*, Springer Lecture Notes in Physics 741, edited by M. Kuster, G. Raffelt, and B. Beltran (Springer Berlin Heidelberg, Berlin, Heidelberg, 2008), pp. 19–50.

[18] P. Sikivie, N. Sullivan, and D. B. Tanner, Phys. Rev. Lett. **112,** 131301 (2014).

[19] M. Lawson, A. J. Millar, M. Pancaldi, E. Vitagliano, and F. Wilczek, Phys. Rev. Lett. **123,** 141802 (2019).

[20] Y. Kim, D. Kim, J. Jeong, J. Kim, Y. C. Shin, and Y. K. Semertzidis, Phys. Dark Universe **26,** 100362 (2019).

[21] Q.-D. Jiang and F. Wilczek, Phys. Rev. B **99,** 125403 (2019).

[22] P. Sikivie, Rev. Mod. Phys. **93,** 015004 (2021).

[23] J. I. McDonald and L. B. Ventura, Phys. Rev. D **101,** 123503 (2020).

[24] M. Chaichian, I. Brevik, and M. Oksanen, Proc. Sci., ICHEP2020 (**2021**) 595 [arXiv:2101.05758].

[25] P. A. Zyla *et al.* (Particle Data Group), Prog. Theor. Exp. Phys. **2020,** 083C01 (2020).

[26] A. Arza, T. Schwetz, and E. Todarello, J. Cosmol. Astropart. Phys. 10 (2020) 013.

[27] P. Carenza, A. Mirizzi, and G. Sigl, Phys. Rev. D **101,** 103016 (2020).

[28] M. Leroy, M. Chianese, T. D. P. Edwards, and C. Weniger, Phys. Rev. D **101,** 123003 (2020).

[29] I. Brevik, M. Chaichian, and M. Oksanen, Eur. Phys. J. C **81,** 926 (2021).

[30] I. Brevik, Universe **7,** 133 (2021).

[31] J. Ouellet and Z. Bogorad, Phys. Rev. D **99,** 055010 (2019).

[32] A. Arza and P. Sikivie, Phys. Rev. Lett. **123,** 131804 (2019).

[33] Z. Qiu, G. Cao, and X.-G. Huang, Phys. Rev. D **95,** 036002 (2017).

[34] J. A. Dror, H. Murayama, and N. L. Rodd, Phys. Rev. D **103,** 115004 (2021).

[35] I. Brevik and M. Chaichian, Eur. Phys. J. C **82,** 202 (2022).

[36] K. Fukushima, S. Imaki, and Z. Qiu, Phys. Rev. D **100,** 045013 (2019).

[37] M. E. Tobar, B. T. McAllister, and M. Goryachev, Phys. Dark Universe **26,** 100339 (2019).

[38] S. Bae, SungWoo Youn, and J. Jeong, Phys. Rev. D **107,** 015012 (2023).

[39] P. Adshead, P. Draper, and B. Lillard, Phys. Rev. D **102,** 123011 (2020).

[40] A. Patkos, Symmetry **14,** 1113 (2022).

[41] M. E. Tobar, B. T. McAllister, and M. Goryachev, Phys. Rev. D **105,** 045009 (2022).

[42] W. DeRocco and A. Hook, Phys. Rev. D **98,** 035021 (2018).

[43] I. H. Brevik and M. M. Chaichian, Int. J. Mod. Phys. A **37,** 22501512 (2022).

[44] J. A. Stratton, *Electromagnetic Theory* (McGraw-Hill Book Company, New York, 1941).

[45] N. G. van Kampen, B. R. A. Nijboer, and K. Schram, Phys. Lett. **26A,** 307 (1968).

[46] Yu. S. Barash and V. L. Ginzburg, in *Electromagnetic Fluctuations and Molecular Forces*, edited by L. V. Keldysh, D. A. Kirzhnitz, and A. A. Maradudin (Elsevier, Amsterdam, 1989), Chap. 6.

[47] K. A. Milton, *The Casimir Effect, Physical Manifestations of Zero-Point Energy* (World Scientific, Singapore, 2001).

[48] M. Zhang, F. Zhang, Y. Ou, J. Cai, and H. Yu, Nanophotonics **8,** 117 (2019).

[49] X. Chen, X. Chen, Z. Wu, Z. Zhang, Z. Wang, L. Heng, S. Wang, Y. Zou, and Z. Tang, J. Phys. D **51,** 285002 (2018).

[50] X. Chen, Z. Zhang, Z. Wang, S. Wang, L. Heng, and Y. Zou, J. Phys. Soc. Jpn. **86,** 104801 (2017).

[51] Y. I. Abdulkarim, A. Mohanty, O. P. Acharya, B. Appasani, M. S. Khan, S. K. Mohapatra, F. F. Muhammadsharif, and J. Dong, Front. Phys. Sec. Optics and Photonics **10,** 359 (2022).